SCIENTIFIC REPORTS

OPEN

Fe_4S_4 Cubane Type Cluster Immobilized on a Graphene Support: A High Performance H_2 Evolution Catalysis in Acidic Water

Received: 9 October 2017
Accepted: 22 November 2017
Published online: 05 December 2017

Ameerunisha Begum[1], Aasif Hassan Sheikh[1], Golam Moula[2] & Sabyasachi Sarkar[2]

The development of alternate catalysts that utilize non-precious metal based electrode materials such as the first row transition metal complexes is an important goal for economic fuel cell design. In this direction, a new Fe_4S_4 cubane type cluster, $[PPh_4]_2[Fe_4S_4(DMET)_4]$ (1) (DMET = cis-1,2-dicarbomethoxyethylene dithiolate) and its composite with functionalized graphene, (1@graphene) have been synthesized and characterized. The presence of nanocrystalline structures on graphene matrix in TEM and SEM images of 1@graphene indicate that the cluster (1) has been immobilized. The composite, 1@graphene evolves H_2 gas from p-toluene sulfonic acid (TsOH) in a mixture of H_2O and CH_3CN under ambient conditions with a significant turnover number of 3200. 1@graphene electro-catalyzes H_2 evolution at E_p, −1.2 V with remarkable throughput, catalytic efficiency and stability in only H_2O or in only CH_3CN. The Fe_4S_4 cluster (1) alone electro-catalyzes hydrogen evolution at E_p, −0.75 V from TsOH in CH_3CN. The X-ray crystal structure of the Fe_4S_4 cluster (1) (λ_{max}, CH_2Cl_2, 823 nm; ε, 2200 $mol^{-1}\,cm^{-1}$) shows that it is dianionic with a cumulative oxidation state of +2.5 for the iron centers and short C-S bond distances (ca., 1.712 Å & 1.727 Å) indicating the presence of sulfur based radicals.

The presence of the dimetallic iron and heterodimetallic iron-nickel centers at the active sites of the hydrogenases has evoked the researchers to search for a non-platinum catalyst material for proton reduction and H_2 splitting. The nanocomposites of hydrogenase mimics with large surface area and versatile electronic behavior are expected to catalyze reduction of protons to hydrogen gas at lower electro-potentials than platinum based electrode materials[1–5]. The three known classes of hydrogenases, [NiFe]−, [FeFe]− and FeS−cluster free hydrogenases contain iron at their active site which is coordinated by thiolates, CO, CN^- or a light sensitive cofactor (Fig. 1a)[6–13]. Electro-catalytic H_2 generation involves reduction of protons to H_2 gas at lower reduction potentials towards E_p, 0.0 V under a catalyst that can performance-wise replace the platinum electrode (i.e., −0.413 V at pH 7.0)[14–21]. Several electro-catalysts for hydrogen evolution have been reported including a series of multinuclear iron sulfur complexes with benzene tetrathiolate bridges, iron carbonyl clusters, cobalt-dithiolene, metallo-porphyrins, low-valent transition metal complexes, diiron dithiolates, multinuclear Fe-S cluster with a $Fe_{cubane}(\mu\text{-SR})Fe_{subsite}$ linkage, molybdenum-sulfur dimers, cobalt glyoximes, substituted iron glyoximes, carbon nanotube grafted nickel bisdiphosphine complexes, and mononuclear iron(II) polypyridyl complexes[22–29].

Nickel(II)− and iron(III) dithiolenes have been reported which electro-catalyze H_2 evolution at potentials comparable to that of platinum disc electrode[30–32]. Recently the research on light driven H_2 production has gained momentum. Biomimetic chalcogels incorporating Fe_4S_4 cubane type clusters linked with $(Sn_2S_{12})^{4-}$ blocks and iron dithiolene complexes have been reported as catalysts for light driven H_2 production from water and as solar fuel catalysts[33,34]. The Fe_4S_4 cubane type cluster take part in many biological electron transfer processes which are also coupled with several other enzymatic reactions. The $6H^+$-$6e^-$ reduction of N_2 to NH_3 by Fe_4S_4 cubane type cluster alone has been reported by van Tamelen *et al.*[35]. Hence, we are interested to find out the efficiency of Fe_4S_4 cubane type cluster alone as electrochemical hydrogen evolution catalysts. Since the Fe_4S_4 cubane type clusters are embedded in protein matrix in the biological active site, the stability and catalytic efficiency of the Fe_4S_4 clusters

[1]Department of Chemistry, Faculty of Science, Jamia Hamdard University, New Delhi, 110062, India. [2]Nanoscience and Synthetic Leaf Laboratory at Downing Hall, Center for Healthcare Science and Technology, Indian Institute of Engineering Science and Technology, Botanic Garden, Howrah, 711103 West Bengal, India. Correspondence and requests for materials should be addressed to A.B. (email: abegum@jamiahamdard.ac.in)

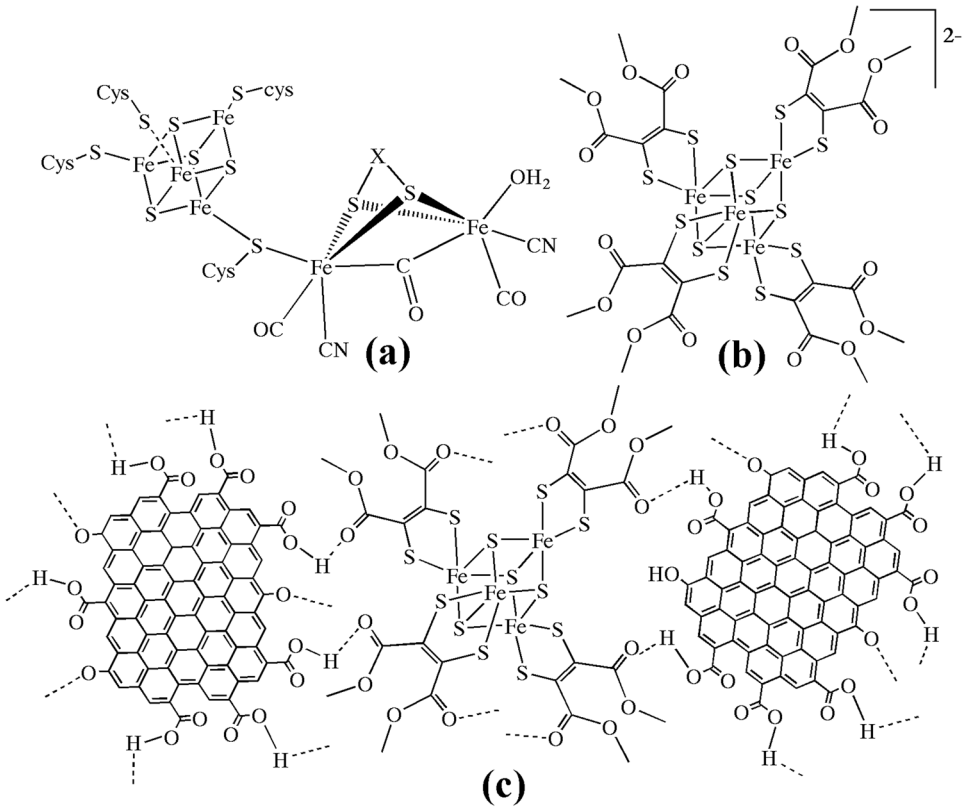

Figure 1. Structures of (**a**) H-cluster in H_2 evolving *Clostridium pasteurianum*[1], (**b**) anionic part of the cluster (**1**), (**c**) H-bonding interactions in **1**@graphene.

might be enhanced if they can be embedded or immobilized on a graphene support. Two dimensional nanomaterials of various compositions including graphene have been studied as catalysts in electrochemical reactions such as hydrogen evolution reaction (HER), oxygen reduction reaction (ORR), oxygen evolution reaction (OER) and carbon dioxide reduction[36]. Recently 2D nanomaterials including functionalized graphene, their hybrids have gained interests in electrochemical energy conversion and storage devices[37]. Defects existing in the 2D nanomaterials play an important role in tailoring of optical and electric properties. Functionalized graphene obtained by oxidation contains –COOH, –C=O, and –OH functional groups which can be used to immobilize metal ions and organic groups. Several graphene-photocatalyst composites have been developed recently for HER[38]. Graphene as a matrix would enhance the catalytic performance of the electrocatalysts embedded on it due to its large surface area, excellent conductivity and indefinite durability. Graphene oxide gets folded to close like fisted form and entraps a large molecule such as tetraphenylporphyrin (TPP)[39]. Several graphene based hybrid electrocatalysts as anodic and cathodic fuel cell electrode materials have been reviewed[40]. Here in we report a new Fe_4S_4 cubane type cluster, $[PPh_4]_2[Fe_4(\mu_3\text{–}S)_4(DMET)_4]$ (**1**, Fig. 1b) and a functionalized graphene composite, **1**@graphene (Fig. 1c) which react with protons and evolve H_2 gas in a mixture of CH_3CN and water under ambient conditions and electrochemically at E_p, −1.21 V in CH_3CN or in H_2O.

Results and Discussion

Synthesis and X-ray structural data of the Fe_4S_4 cubane type cluster, $[PPh_4]_2[Fe_4(\mu_3\text{-}S)_4(DMET)_4]$ (1).

The cluster (**1**) was prepared by the reaction of iron(II) polysulfide, $[PPh_4]_4[Fe_2^{II}S_{12}]$ with dimethylacetylene dicarboxylate (DMAD) and lithium sulfide (Li_2S) in CH_3CN under Schlenk conditions. The X-ray structure determination of (**1**) indicates the presence of dianionic, $[Fe_4(\mu_3\text{-}S_4)(DMET)]^{2-}$ cluster and $[PPh_4]$ cations in 1:2 ratio. The ORTEP view of the anionic part of the cluster (**1**) is shown in Fig. 2 which confirms the formation of Fe_4S_4 core with four bidentate DMET ligands coordinated to iron. The geometry around each iron atom is square pyramidal formed by three inorganic sulfurs (S^{2-}) and two thiolates of the DMET ligand. The Fe–S bond lengths are similar at all iron centers, (Fe(1) and Fe(2)) and in the range 2.156 Å–2.250 Å. This is in contrast to the longer Fe-S bond distances (2.246 Å–2.383 Å) in the tetra anionic, super reduced cluster, $[NBu_4]_4[Fe_3^{III}Fe^{II}(\mu_3\text{-}S)_4(mnt)_3^{6-}(mnt)^{1-\cdot}]^{4-\cdot}$ (**2**) (mnt = maleonitrile dithiolate)[32]. The Fe…Fe separations (Fe–Fe, 2.695 Å and 2.722 Å) are remarkably shorter in the cluster (**1**) in contrast to those observed in (**2**) (Fe-Fe, 2.843 Å–3.123 Å) and four of the C–S bond distances (S(2)–C(2) & S(2A)–C(2A), 1.718 Å and S(6)–C(8) & S(6A)–C(8A), 1.721 Å) are considerably shorter in (**1**) indicating oxidation of the dithiolene ligands to their monoanionic form containing sulfur based radicals. The lattice packing in the crystals of (**1**) indicates that the anionic Fe_4S_4 cluster is fully covered by a group four $[PPh_4]$ cations with considerably short S^{2-}(cluster)…H–C(phenyl) (2.91 Å and 3.45 Å) and O(cluster)…H–C(phenyl), (2.43 Å). All of the four S^{2-} in the anionic part are involved in short contacts with C-H

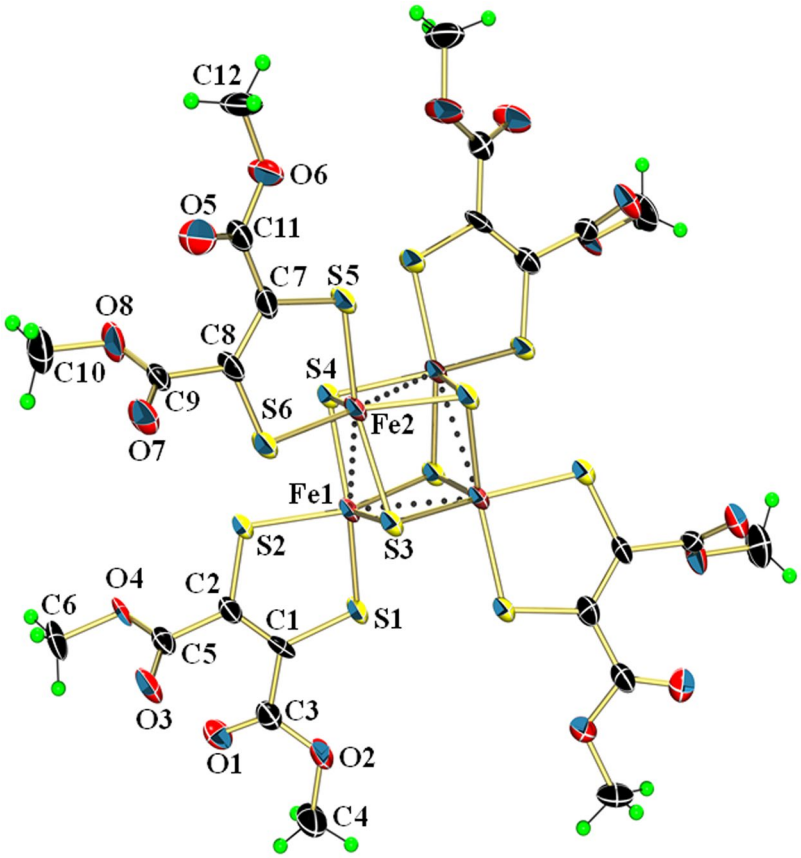

Figure 2. Perspective view of the anionic part of the cluster (**1**) in 50% probability thermal ellipsoids (hydrogen green; carbon, black; oxygen, red; sulfur, yellow; iron, brown). Selected bond lengths (Å): Fe(1)-S(1), 2.1830(15); Fe(1)-S(2), 2.2009(15); Fe(1)-S(3), 2.2429(15); Fe(1)-S(4), 2.1574(15); Fe(2)-S(3), 2.1563(15); Fe(2)-S(4), 2.2393(15); Fe(2)-S(5), 2.2037(15); Fe(2)-S(6), 2.1918(15); Fe(1)-Fe(2), 2.6947(11); Fe(2)-Fe(1), 2.7226(11); S(2)-C(4), 1.712(5); S(6)-C(10), 1.727(5).

of the PPh_4 cations. These interactions might provide stability to the cluster skeleton and are reminiscent of the intermolecular interactions observed in native proteins.

The dianionic 1,2-dithiolenes coordinated to metal complexes are known to undergo oxidation resulting in monoanionic ligands with S–based radicals[41–47]. The considerably shorter C−S bond distances in a previously reported $[Fe_4(\mu\text{-}S)_4(S_2C_2(CF_3)_2)_4]^{2-}$ dianion and in cluster (**1**) indicate that the four monoanionic dithiolates provide only four negative charges to the cluster whereas the four inorganic sulfurs (S^{2-}) provide eight negative charges making up a total of 12 negative charges which are satisfied by the four iron ions and two $[AsPh_4]/[PPh_4]$ cations[48,49]. This confirms that the four iron centers are in a comprehensive oxidation state of +2.5 and the four dithiolene ligands have been oxidized to form monoanionic ligands with four S-based radicals. The appearance of a peak at m/z, 1514 in electro spray ionization mass spectrum (Fig. 3) indicates the stability of $\{[PPh_4][Fe_4(\mu_3\text{–}S)_4(DMET)_4]\}^-$ complex ion in CH_3CN. The complex (**1**) is EPR silent both in the solid state and in CH_2Cl_2 solution. The diamagnetic nature of the cluster (**1**) is understood from the room temperature magnetic moment (μ_{eff}) of $<1\ \mu_B$. The presence of a band around λ, 823 nm (ε, 2200 $M^{-1}cm^{-1}$) in the electronic spectrum of (**1**) in CH_2Cl_2 (Fig. 3) can be assigned to an intervalence-charge transfer (IVCT) band which is observed in sulphur based radical containing complexes. This indicates the presence of S–based radicals and since the complex (**1**) is diamagnetic, the S-based radicals are expected to be coupled.

Synthesis and characterization of the composite, 1@graphene. The composite, **1**@graphene was prepared by the ultrasonication of Fe_4S_4 cubane type cluster, (**1**) and functionalized graphene for 10 h in CH_3CN-H2O under an argon atmosphere. It was then evapourated to dryness and the black residue was labelled as **1**@graphene. The IR spectral peaks of **1**@graphene show significant shifts to lower frequencies compared with the Fe_4S_4 cluster (**1**). The doublet at 1718 cm^{-1} and 1690 cm^{-1} observed in (**1**) due to –COO stretching of dithiolenes is shifted to 1616 cm^{-1} and 1610 cm^{-1} in **1**@graphene and the doublet is also broadened (Supplementary information). This indicates the existence of the H-bonding interactions with –COOH of the f-graphene as shown in Fig. 1c. Furthermore, in **1**@graphene, a broad band is observed at 3324 cm^{-1} indicating the presence of hydrogen bonded –OH groups. Functionalized graphene and the composite, **1**@graphene were further analyzed by scanning electron microscopy (SEM) and results are displayed in Fig. 4. The sample containing functionalized graphene displayed transparent and thin filmy structures as shown in the Fig. 4A and B. The sample containing

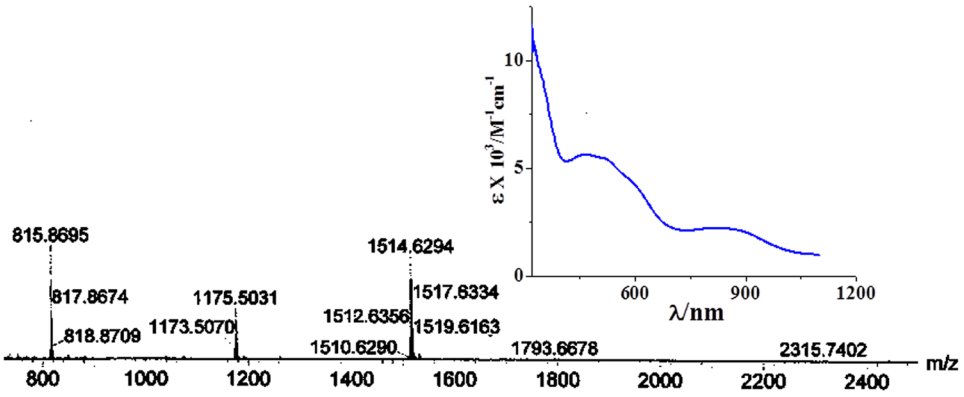

Figure 3. ESI-MS (negative) of the cluster (**1**) in CH_3CN. (Inset: UV-VIS spectrum of (1) in CH_2Cl_2.

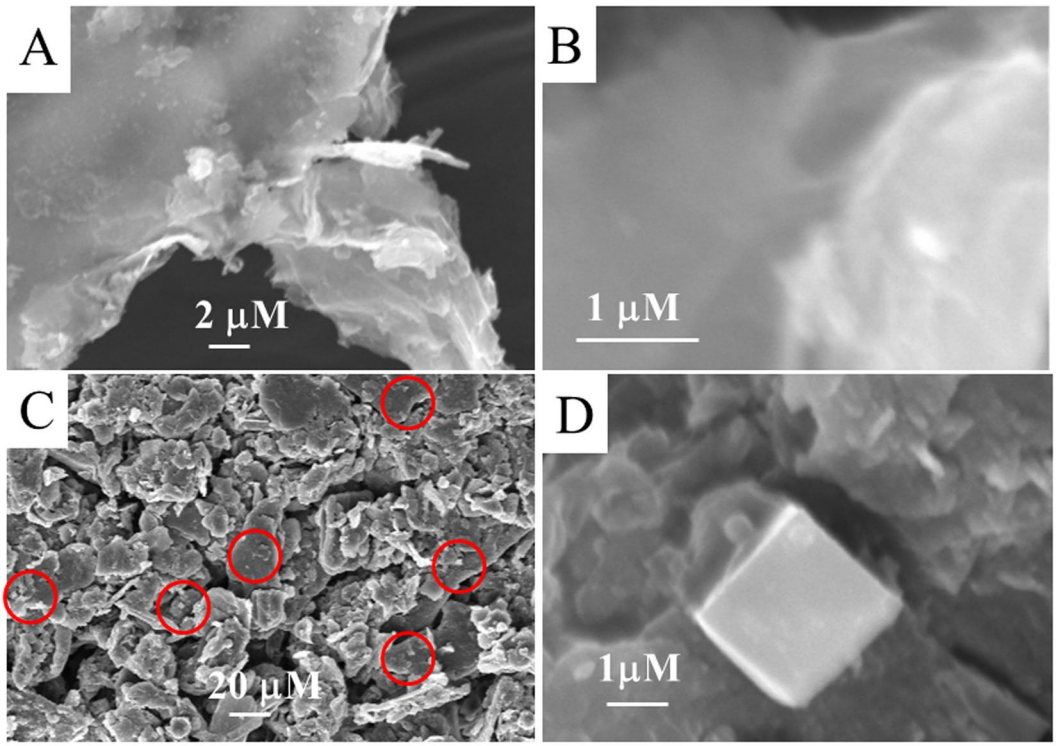

Figure 4. (**A** and **B**) SEM images of the functionalized graphene at low and higher magnifications on aluminium matrix. (**C** and **D**) SEM images of 1@graphene at low and higher magnifications on aluminium matrix. C, red circled area is magnified in D displaying the Fe_4S_4 cubane type cluster, 1 embedded in a bed of functionalized graphene.

1@graphene diaplayed a mixture of graphene and the Fe_4S_4 cubane type cluster (**1**) as shown in Fig. 4C (low magnification) and Fig. 4D (higher magnification). The red circled area in Fig. 4C has been magnified and shown in Fig. 4D which indicates that a cubic structure is embedded in a bed of transparent filmy structure. The functionalized graphene, Fe_4S_4 cluster (**1**) and the composite **1**@graphene were dispersed in H_2O-CH_3CN, deposited onto carbon coated copper grids and analyzed by HR TEM. The results are displayed in Fig. 5 which indicates that the functionalized graphene solidifies as a film whereas the Fe_4S_4 cluster recrystallize as nanocrystals. The TEM images of **1**@graphene displayed in Fig. 5C and D indicated the presence of dark crystals/particles of Fe_4S_4 cluster on the graphene matrix. The Fe_4S_4 crystals can be immobilized on a functionalized graphene matrix through H-bonding interactions with the –COOH, -OH functional groups which has also been corroborated by IR spectral studies as described above. Because the Fe_4S_4 cubane type clusters crystallize in the form of nanocubes and microcubes as confirmed by our unpublished results on the cluster, $[NBu_4]_4[Fe_3^{III}Fe^{II}(\mu_3\text{–}S)_4(mnt)_3^{6-}(mnt)^{1-\cdot}]^{4-\cdot}$ (**2**) which displays nanocubes on recrystallization from CH_3CN on a brass matrix and as nanotriangles on recrystallization from ethanol on a brass matrix. The EDX analysis of these nanocubes and nanotriangles confirmed the presence of carbon, iron, sulphur, phosphorous in the expected ranges as described in our unpublished results.

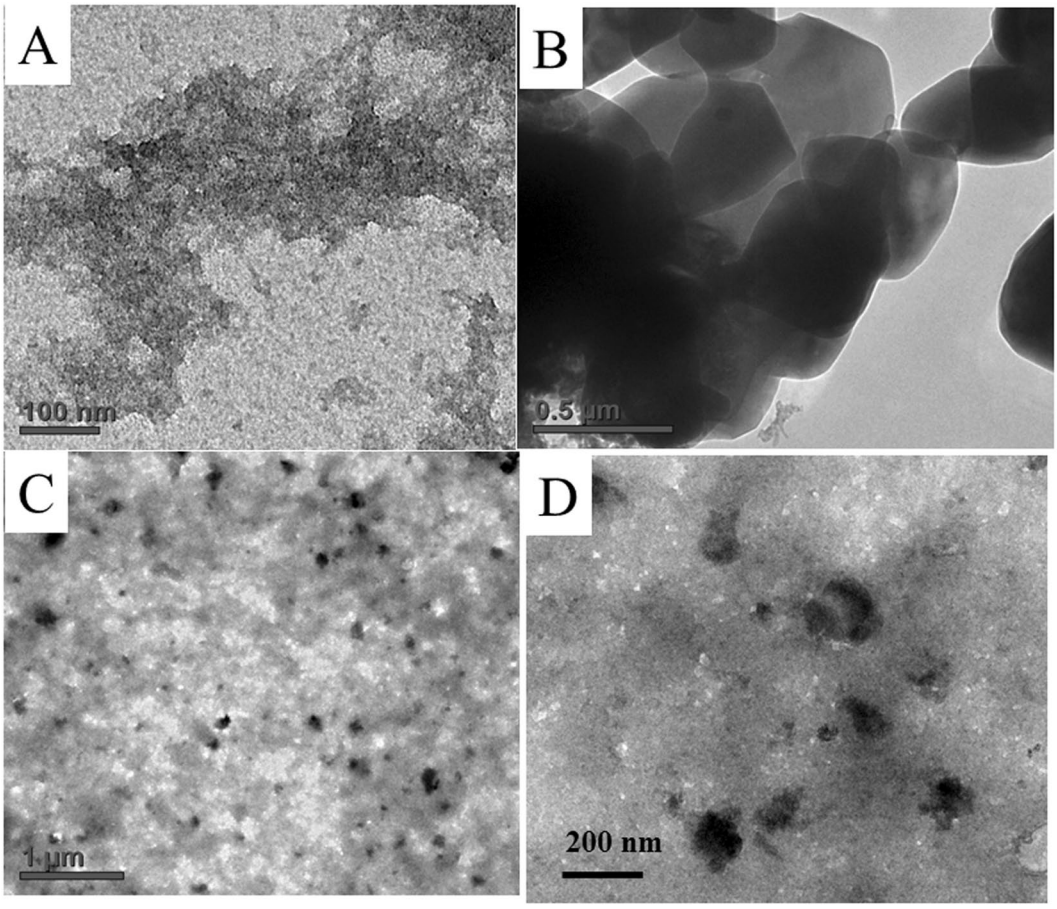

Figure 5. HR TEM images of f-graphene, Fe_4S_4 cluster (**1**) and **1**@graphene in CH_3CN-H_2O on carbon coated copper grids. (**A**) functionalized graphene. (**B**) Fe_4S_4 cluster (1). (**C** and **D**) **1**@graphene at low and high magnifications.

Cyclic voltammetric data and proton reduction. The Fe_4S_4 cubane type cluster (**1**) undergoes three reversible one electron redox processes around $E_{1/2}$, +0.45 V, +0.11 V and −0.49 V (ΔE, 60 mV) and two quasi-reversible redox processes around E, −1.01 V and −1.22 V in CH_2Cl_2 (Fig. 6). The waves at E, −0.49 V, −1.01 V and −1.22 V can be assigned to the DMET ligand based redox processes since these were observed also in other related iron(III) dithiolene complexes and a nickel(II) complex of the DMET ligand[30–32]. The reversible redox process occurring near zero ($E_{1/2}$, +0.107 V) can be assigned to Fe^{3+}/Fe^{2+} and the one occurring at $E_{1/2}$, +0.45 V can be assigned to Fe^{2+}/Fe^{3+} redox process. These assignments of the redox waves of the cluster (**1**) have been done based on comparison of cyclic voltammetric profiles of various Fe_4S_4 clusters, iron(II)/iron(III) and nickel(II)complexes of similar dithiolene ligands including classical tetrahedral Fe_4S_4 clusters of Holm *et al.*[50–59].

The complex (**1**) electro-catalyzes hydrogen evolution from *p*-toluene sulfonic acid (TsOH) in CH_3CN. On addition of TSOH (0.25 M, 0.05 ml) to the cluster (**1**) in CH_3CN, the negative current at potential E, −0.72 V was increasing as shown in Fig. 6B. But the reversible redox couples around E_p, +0.445 V and Ep, +0.107 V were unaffected by the addition of TsOH. This indicates that the preferential sites of protonation could be the sulfur donors of the radical containing monoanionic dithiolate. The increase in current is due to the reduction of TsOH protons followed by the evolution of hydrogen gas. Controlled potential electrolysis of a mixture of the cluster (**1**) (0.025 mmol) and TsOH (0.25 mmol) was carried out in CH_3CN at E_p, −0.8 V. A net charge of 29 mC passed over a period of 2 minutes. Head space analysis of the electrochemical cell by gas chromatography confirmed the presence of H_2 gas. The cluster (**1**, 0.025 mmol) consumed 0.25 mmol of TsOH and the TON (turnover number) of (**1**) in CH_3CN is 400. The H_2 evolution occurring at E_p, −0.8 V using TsOH is proposed to be promoted by a S-radical based process. The iron bound monoanionic dithiolate type S-donor sites of DMET can be protonated upon addition of TSOH and reduce protons to H_2 on application of electric potential. In the process, the monoanionic dithiolate S- donors can in turn get oxidized to a fully oxidized, neutral di-radical ligand. The reduction of protons coupled to the oxidation of monoanionic dithiolate to neutral di-radical ligand is modulated by the iron center. Because similar DMET complexes of several other transition metal ions do not catalyze proton reduction at such a low reduction potential, *viz*., E_p, 0.72 V.

The cyclic voltammogram of the composite, **1**@graphene is similar to that of the cluster (**1**) as shown in Fig. 7A. It displays three reversible one electron redox processes at E_p, −0.41 V, +0.23 V and +0.57 V in CH_3CN which are assigned to S-radical based Fe^{2+}/Fe^{3+} redox processes as described above for the pure cluster in CH_2Cl_2 (*vide supra*).

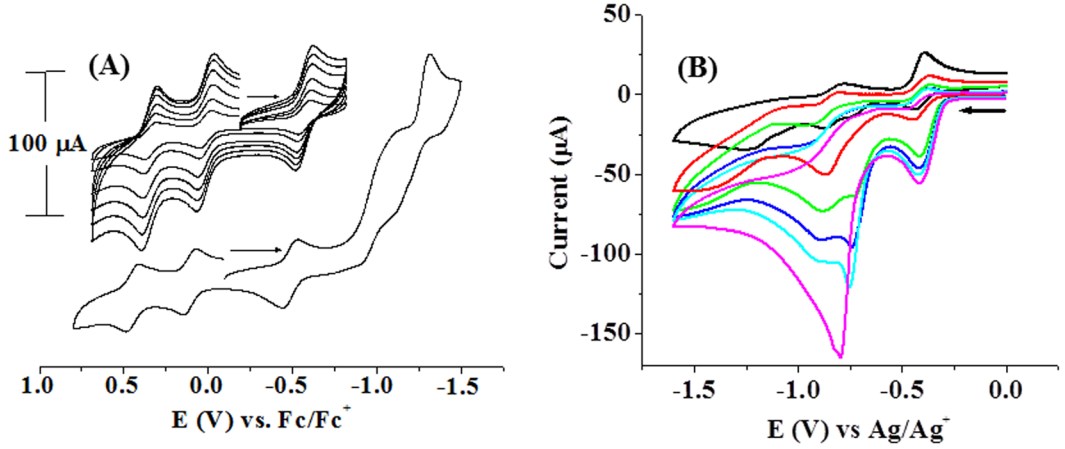

Figure 6. (**A**) Cyclic voltammogram of (1) (1 mM) in CH_2Cl_2 (Supporting electrolyte, NBu_4ClO_4 (0.2 M), GCE working, Pt wire auxillary and Ag/AgCl reference electrodes). Inset, reversible redox couples at different scan rates, 50–500 mV/sec. (**B**) Cyclic voltammograms of the cluster (1) (0.025 mM, black) in CH_3CN as a function of increasing concentrations of added *p*-TsOH (0.25 M, 0.05 ml additions each) at a scan rate of 100 mVs^{-1}. Supporting electrolyte, NBu_4PF_6 (0.2 M), GCE working, Pt wire auxillary and Ag/AgCl reference electrodes.

The composite, **1**@graphene electrocatalyzes TsOH-proton reduction to H_2 at E_p, −1.19 V in CH_3CN as a solvent. On addition of 0.4g of TsOH (2 mmol in 2 mL CH_3CN), overall current of −0.95 mA passed at E, −1.19 V. The increase in current as a function of added TsOH solutions in CH_3CN (1 M, 0.1 ml each) are shown in Fig. 7B and for clarity only the forward scans are displayed in Fig. 7C. The composite electrocatalyzes the above mentioned reduction to H_2 at the same potential, E_p, −1.2 V in water as a solvent with better catalytic efficiency and higher current output. On addition of 0.1 g of TsOH (0.5 mmol in 1 mL H_2O), overall current of −3.15 mA passed at E, −1.2 V as shown in Fig. 7D and for clarity only the forward scans are displayed in Fig. 7E. The composite (0.05 g, 0.025 mmol with respect to Fe_4S_4 cubane cluster, **1**) consumed 2 mmol of TsOH with a turnover number of 3200. Formation of bubbles and brisk effervescence were observed upon addition CH_3CN (1mL) to the electrochemical cell containing the composite **1**@graphene and TsOH in water. This was confirmed to be H_2 gas by head space analysis by gas chromatography[30]. The stability of the Fe_4S_4 cubane type cluster and its composite, **1**@graphene are confirmed in de-aerated water under argon due to the insolubility of (**1**) in water. The cluster (**1**) was extracted from the composite after cyclic voltammetric experiments by ultrasonication in CH_3CN followed by centrifugation and evapouration to dryness. The elemental analysis of the residue indicated the presence of carbon, hydrogen, nitrogen and sulphur according to the percentage elemental composition of the cluster (**1**). The composite, **1**@graphene isolated from water medium displayed an ESI-MS (−ve) signal at m/z, 1514. The IR spectrum of **1**@graphene after catalysis is dominated by peaks due to ν_{NO3} (KNO_3, supporting electrolyte) and $\nu_{S=O}$ (tosic acid) stretching at 1371 cm^{-1}, 1177 cm^{-1} and 1120 cm^{-1}. But weak signals at 1720 & 1644 cm^{-1} (-COO of dithiolene) and at 1528 & 1490 cm^{-1} (-C=C- of dithiolene) coupled with the elemental analytical data indicate that the Fe_4S_4 cluster is intact. The cluster@graphene is confirmed to be stable in the solid state in water where as it is prone for attack only when it is dissolved in CH_3CN or even in a mixture of H_2O-CH_3CN. This is due to the fact that in CH_3CN, the composite functions as an emulsion of graphene in the CH_3CN solution of (**1**) where as in water, it is an emulsion in graphene solution. The composite remains intact with indefinite durability and it is well behaved in pure water. But in a mixture of H_2O-CH_3CN, both the cluster (**1**) and graphene get into solution. The composite, **1**@graphene shows an enhanced catalytic activity (TON, 3200) as compared to the pure Fe_4S_4 cluster (**1**) alone (TON, 400). This could be due to *in situ* reduction of the oxidized Fe_4S_4 cluster by graphene. As much as the cluster (**1**) gets oxidized after proton reduction, that much can be reduced on the graphene matrix immediately. The graphene matrix can function similar to an external sacrificial electron donor[60]. Only graphene in the absence of the Fe_4S_4 cubane type cluster electrocatalyzes proton reduction at a higher negative potential, *ca.*, −1.7 V as shown in Fig. 7F. But the catalysis onsets at the reduction potential, *ca.* Ep, −0.41 V itself. Under similar experimental conditions, only TsOH, did not show any response on a GCE in the potential range, E, 0.0 V to −1.8 V (supporting information).

In summary, an ideal catalytic material for the reduction of TsOH protons to H_2 gas in water has been achieved by immobilizing the Fe_4S_4 cubane type cluster, $[PPh_4]_2[Fe_4S_4(DMET)_4]$ (**1**) on a functionalized graphene support. A high current output (3200 TON) and an extreme stability of the catalytic material in water was concluded from the cyclic voltammetric and ESI-MS experiments. Only Fe_4S_4 cluster, (**1**) electrocatalyzes the same reduction reaction with low catalytic efficiency (400 TON) and concomitant decomposition to dimeric compound, $[PPh_4]_2[Fe^{III}(DMET)_2]_2$. The Fe_4S_4 cubane type cluster was synthesized in a novel synthetic route and structurally characterized. The cluster (**1**) is EPR silent and it displays reversible, one electron redox waves around $E_{1/2}$, +0.107 V and at +0.45 V) which could be assigned to the Fe^{3+}/Fe^{2+} and Fe^{2+}/Fe^{3+} redox processes.

Methods

Synthesis of $[PPh_4]_2[Fe_4S_4\{S_2C_2(COOCH_3)_2\}_4]$ (1). The reaction was done under Schlenk conditions. Acetonitrile (40 ml) was purged with argon gas for 30 min. and iron(II)-polysulfide, $[PPh_4]_4[Fe^{II}{}_2S_{12}]$ (Electronic Supplementary information) (0.500 g) was added into it. The suspension was stirred for 20 min. followed by the addition of dimethyl acetylene carboxylate (0.5 ml) and freshly purchased lithium sulfide (Li_2S, 0.15 g) under

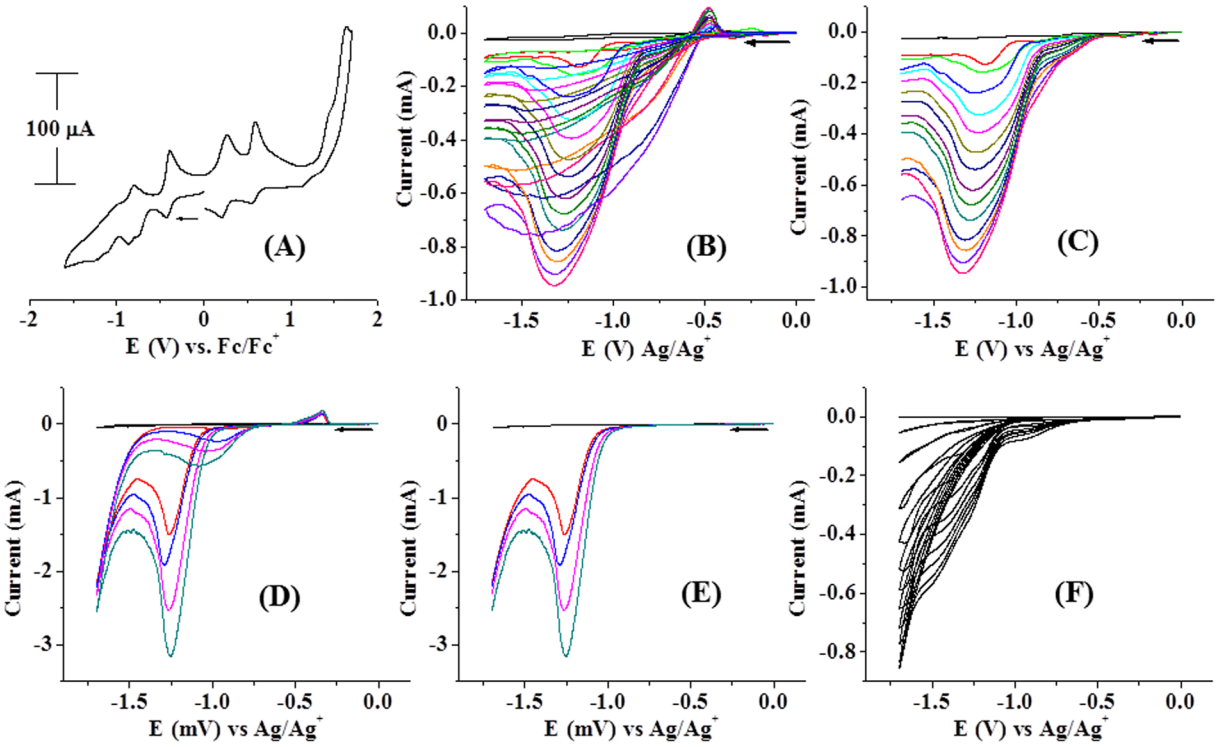

Figure 7. (**A**) Cyclic voltammogram of the graphene composite (**1**@graphene) (1 mM) in CH_3CN scan rate of 100 mVs^{-1} (Supporting electrolyte, NBu_4PF_6/CH_3CN or KNO_3/H_2O (0.2 M), GCE working, Pt wire auxillary and Ag/AgCl reference electrodes). (**B**) Cyclic voltammograms as a function of increasing concentrations of added *p*-TsOH in CH_3CN. (0.5 M *p*-TsOH, 0.1 mL each in CH_3CN), (**C**) Displaying only forward reduction waves for clarity, (**D**) 0.5 M *p*-TsOH, 0.1 mL each in water, (**E**) Displaying only forward reduction waves for clarity, (**F**) Addition of 0.5 M *p*-TsOH, 0.1 mL each in CH_3CN to functionalized graphene only.

argon. The black colored reaction mixture was stirred for 8h at room temperature and then diethylether (100 ml) was added. The reaction flask was closed tightly and allowed to stand at 10 °C for two days under argon. Dark green crystals were formed which were filtered and stored under argon. Dark green single crystals suitable for X-ray diffraction were obtained by layering of diethylether onto acetonitrile solution of the complex under argon. Data for (**1**): Yield, 0.6 g, C, H, N elemental analysis calculated for $[PPh_4]_2[Fe_4S_4\{S_2C_2(COOCH_3)_2\}_4].2H_2O$, C, 45.72, H, 3.62; Found, C, 45.53, H, 3.82. ESI-MS (negative) in CH_3CN; m/z, 1514 $\{[PPh_4][Fe_4^{III}(\mu_3\text{–}S)_4(S_2C_2(COOCH_3)_2)_4]\}^-$; ESI-MS (positive), m/z, 339 $[PPh_4]^+$. FT-IR (KBr disc, cm^{-1}): 3400(br), 2945(m), 1714 (s), 1693 (s), 1433(s), 1238 (s), 1212 (m), 1084 (m), 995(m), 722 (s), 688 (s), 526(s) (br, broad, w, weak, m, medium, s, strong). UV-visible in CH_2Cl_2 [λ/nm ($\varepsilon/M^{-1}cm^{-1}$)]: 823 (2200), 582 (4500), 467 (5600). EPR silent, $\mu_{eff} = 0.8\ \mu_B$ at 298K. E ½ = +0.445 V ($\Delta E = 60$ mV), +0.107 V ($\Delta E = 60$ mV) and −0.494 V ($\Delta E = 60$ mV) vs. Ag/AgCl; E, (quasi-reversible), −1.005 V and −1.219 V vs. Ag/AgCl in CH_2Cl_2-0.2M NBu_4ClO_4 with GC working electrode.

Preparation of functionalized grapheme. Graphite powder (0.5 g) was taken in THF (80 mL) and water (20 mL), stirred at 38 C for 2 h and ultra-sonicated for 10 h. The solvents were decanted after centrifugation and the residue was dried thoroughly. This residue was treated carefully dropwise with concentrated H_2SO_4 (30 mL) and fuming nitric acid (10 mL) at 0 °C. The reaction mixture was heated under reflux for 12 h and allowed to stand at 38 °C for 10 h. The supernatant acid layer was decanted and the residue was washed thoroughly with water by centrifugation and dried. FT-IR (ν, cm^{-1}): 1718 (br.), 1600 (w).

Preparation of the Composite, 1@graphene. The Fe_4S_4 cubane type cluster (**1**, 0.05 g) in degassed LC-MS grade CH_3CN (12 mL) was mixed with functionalized graphene (0.05 g) in degassed LC-MS grade H_2O (8 mL) and ultra-sonicated in closed sample vial under argon atmosphere for 3 h. The reaction mixture was evaporated to dryness and the residue was used in catalytic experiments. FT-IR (ν, cm^{-1}): 3324(br.), 1616 (br.), 1610 (w), 1433(w), 1364 (w), 1233 (w), 1103 (m), 997 (m) 751 (w), 593 (w).

X-ray crystallographic measurement of (1). The dark green single crystals of the complex (**1**) were obtained by layering of diethylether onto acetonitrile solution of the complex under argon and isolated as $[PPh_4]_2[Fe_4^{III}(\mu_3\text{–}S)_4(DMET)_2^{4-}((DMET)^{1-\cdot})_2]^{2-}.(CH_3CH_2)_2O.2H_2O$. The intensity data for single crystals of (**1**) was collected at 120 K on a Bruker AXS Smart APEX CCD diffractometer with graphite monochromated MoK_α radiation (0.71073 Å). Data reduction and absorption corrections were done using SAINTPLUS program package. The structure was solved by direct and conventional Fourier methods and refined on F^2 by full-matrix

least-squares technique using SHELXTL program package[61]. All non-hydrogen atoms were refined anisotropically, H atoms at idealized positions in riding mode. structure data for (**1**): $C_{76}H_{64}Fe_4O_{19}P_2S_{12}$, Mr = 1951.33, Monoclinic, P2/c, a = 13.541(5), b = 13.376(5), c = 24.923(5) (Å), β = 98.859(5)°, Volume = 4460(3) Å3, Z = 4, ρ_{calcd} = 1.453 Mg/m3, μ(MoKα) = 1.018 mm^{-1}, F(000) = 1996, Unique reflections, 22403 at 120 K, Observed reflections, 7840, Parameters, 503, GOF = 1.034, R1 = 0.0632, wR2 = 0.1796. CCDC-871183 of the complex (**1**) can be downloaded from Cambridge crystallographic data center.

References

1. Adams, M. W. W. & Stiefel, E. I. Biological hydrogen production: not so elementary. *Science* **282**, 1842–1843 (1998).
2. Tard, C. & Pickett, C. J. Structural and functional analogues of the active sites of the [Fe]-, [NiFe]-, and [FeFe]-hydrogenases. *Chem. Rev.* **109**, 2245–2274 (2009).
3. Thoi, V. S., Sun, Y., Long, J. R. & Chang, C. J. Complexes of earth-abundant metals for catalytic electrochemical hydrogen generation under aqueous conditions. *Chem. Soc. Rev.* **42**, 2388–2400 (2013).
4. Gloaguen, F. & Rauchfuss, T. B. Small molecule mimics of hydrogenases: Hydrides and redox. *Chem. Soc. Rev*. **38** (2009).
5. Rakowski-DuBois, M. & DuBois, D. L. The roles of the first and second coordination spheres in the design of molecular catalysts for H_2 production and oxidation. *Chem. Soc. Rev.* **38**, 62–72 (2009).
6. Best, S. P. Spectroelectrochemistry of hydrogenase enzymes and related compounds. *Coord. Chem. Rev.* **249**, 1536–1554 (2005).
7. De Lacey, A. L., Fernandez, V. M., Rousset, M. & Cammack, R. Activation and Inactivation of Hydrogenase Function and the Catalytic Cycle: Spectroelectrochemical Studies. *Chem. Rev.* **107**, 4304–4330 (2007).
8. Lubitz, W., Reijerse, E. & van Gastel, M. [NiFe] and [FeFe] hydrogenases studied by advanced magnetic resonance techniques. *Chem. Rev.* **107**, 4331–4365 (2007).
9. Fontecilla-Camps, J. C., Volbeda, A., Cavazza, C. & Nicolet, Y. Structure/Function relationships of [NiFe]- and [FeFe]-hydrogenases. *Chem. Rev.* **107**, 4273–4303 (2007).
10. Kubas, G. J. Fundamentals of H_2 binding and reactivity on transition metals underlying hydrogenase function and H_2 production and storage. *Chem. Rev.* **107**, 4152–4205 (2007).
11. Peters, J. W., Lawzilotta, W. N., Lemon, B. J. & Seefeldt, L. C. X-ray crystal structure of the Fe-only hydrogenase (CpI) from *Clostridium pasteurianum* to 1.8 angstrom resolution. *Science* **282**, 1853–1858 (1998).
12. Volbeda, A. *et al*. Crystal structure of the nickel–iron hydrogenase from Desulfovibrio gigas. *Nature* **373**, 580–587 (1995).
13. Shima, S. *et al*. The cofactor of the iron–sulfur cluster free hydrogenase Hmd: structure of the light-inactivation product. *Angew. Chem. Int. Ed.* **43**, 2547–2551 (2004).
14. Gloaguen, F., Lawrence, J. D. & Rauchfuss, T. B. Biomimetic hydrogen evolution catalyzed by an iron carbonyl thiolate. *J. Am. Chem. Soc.* **123**, 9476–9477 (2001).
15. Mejia-Rodriguez, R., Chong, D., Reibenspies, J. H., Soriaga, M. P. & Darensbourg, M. Y. The hydrophilic phosphatriazaadamantane ligand in the development of $_H$2 production electrocatalysts: iron hydrogenase model complexes. *J. Am. Chem. Soc.* **126**, 12004–12014 (2004).
16. Borg, S. J. *et al*. Electron Transfer at a Dithiolate-Bridged Diiron Assembly: Electrocatalytic Hydrogen Evolution. *J. Am. Chem. Soc.* **126**, 16988–16999 (2004).
17. Ott, S., Kritikos, M., Akermark, B., Sun, L. & Lomoth, R. A. Biomimetic Pathway for Hydrogen Evolution from a Model of the Iron Hydrogenase Active Site. *Angew. Chem. Int. Ed.* **43**, 1006–1009 (2004).
18. Wilson, A. D. *et al*. Agostic interaction and intramolecular proton transfer from the protonation of dihydrogen ortho metalated ruthenium complexes. *Proc. Natl. Acad. Sci. USA* **104**, 6945–6950 (2007).
19. Hu, X., Brunschwig, B. S. & Peters, J. C. Electrocatalytic Hydrogen Evolution at Low Overpotentials by Cobalt Macrocyclic Glyoxime and Tetraimine Complexes. *J. Am. Chem. Soc.* **129**, 8988–8998 (2007).
20. Le Goff, A. *et al*. From hydrogenases to noble metal-free catalytic nanomaterials for H2 production and uptake. *Science* **326**, 1384–1387 (2009).
21. Kaur-Ghumann, S., Schwartz, L., Lomoth, R., Stein, M. & Ott, S. Catalytic hydrogen evolution from mononuclear iron(II) carbonyl complexes as minimal functional models of the [FeFe] hydrogenase active site. *Angew. Chem. Int. Ed.* **49**, 8033–8036 (2010).
22. Chen, L. *et al*. Multielectron-transfer templates via consecutive two-electron transformations: iron–sulfur complexes relevant to biological enzymes. *Chem. Eur. J.* **18**, 13968–13973 (2012).
23. Fourmond, V., Jacques, P.-A., Fontecave, M. & Artero, V. H_2 Evolution and molecular electrocatalysts: determination of overpotentials and effect of homoconjugation. *Inorg. Chem.* **49**, 10338–10347 (2010).
24. Rail, M. D. & Berben, L. A. Directing the reactivity of $[HFe_4N(CO)_{12}]^-$ toward H^+ or CO_2 reduction by understanding the electrocatalytic mechanism. *J. Am. Chem. Soc.* **133**, 18577–18579 (2011).
25. Rose, M. J., Gray, H. B. & Winkler, J. R. Hydrogen generation catalyzed by fluorinated diglyoxime–iron complexes at low overpotentials. *J. Am. Chem. Soc.* **134**, 8310–8313 (2012).
26. McNamara, W. R. *et al*. Cobalt–dithiolene complex for the photocatalytic and electrocatalytic reduction of protons. *J. Am. Chem. Soc.* **133**, 15368–15371 (2011).
27. Nomura, M., Fujita-Takayama, C., Yagisawa, T., Sugiyama, T. & Kajitani, M. An organometallic dithiolene complex exhibiting electrochemically initiated hydrogen generation. *Dalton Trans.* **42**, 4764–4767 (2013).
28. Chen, L. *et al*. Tetranuclear iron complexes bearing benzenetetrathiolate bridges as four-electron transformation templates and their electrocatalytic properties for proton reduction. *Inorg. Chem.* **52**, 1798–1806 (2013).
29. Connor, G. P., Mayer, K. J., Tribble, C. S. & McNamara, W. R. Hydrogen evolution catalyzed by an iron polypyridyl complex in aqueous solutions. *Inorg. Chem.* **53**, 5408–5410 (2014).
30. Begum, A., Moula, G. & Sarkar, S. Nickel(II)–sulfur-based radical-ligand complex as a functional model of hydrogenase. *Chem. Eur. J.* **16**, 12324–12327 (2010).
31. Begum, A. & Sarkar, S. An iron(III) dithiolene complex as a functional model of iron hydrogenase. *Eur. J. Inorg. Chem*. 40–43 (2012).
32. Begum, A., Moula, G., Bose, M. & Sarkar, S. Super reduced Fe_4S_4 cluster of Balch's dithiolene series. *Dalton Trans.* **41**, 3536–3540 (2012).
33. Lv, H. *et al*. Catalytic light-driven generation of hydrogen from water by iron dithiolene complexes. *J. Am. Chem. Soc.* **138**, 11654–11663 (2016).
34. Shim, Y. *et al*. Tunable biomimetic chalcogels with Fe_4S_4 cores and $[S_{nn}S_{2n+2}]^{4-}$ (n = 1, 2, 4) building blocks for solar fuel catalysis. *J. Am. Chem. Soc.* **135**, 2330–2337 (2013).
35. Van Tamelen, E. E., Gladysz, J. A. & Brulet, C. R. Biological and abiological nitrogen fixation by molybdenum bound N_2/4Fe-4S cluster systems. *J. Am. Chem. Soc.* **96**, 3020–3021 (1974).
36. Tan, C. *et al*. Recent advances in ultrathin two-dimensional nanomaterials. *Chem. Rev.* **117**, 6225–6331 (2017).
37. Khan, A. H. *et al*. Two-dimensional (2D) nanomaterials towards electrochemical nanoarchitectonics in energy-related applications. *Bull. Chem. Soc. Jpn.* **90**, 627–648 (2017).
38. Gong, X., Liu, G., Li, Y., Wai Yu, D. Y. & Teoh, W. Y. Functionalized-graphene composites: Fabrication and application in sustainable energy and environment. *Chem. Mater.* **28**, 8082–8118 (2016).

39. Pakhira, B. *et al*. Extraction of preformed graphene from coal: Its clenched fist form entrapping large molecules. *RSC Adv.* **5**, 89076–89082 (2015).
40. Liu, M., Zhang, R. & Chen, W. Graphene-supported nanoelectrocatalysts for fuel cells: Synthesis, properties and applications. *Chem. Rev.* **114**, 5117–5160 (2014).
41. Ghosh, P. *et al*. Coordinated o-dithio- and o-iminothiobenzosemiquinonate(1−) π radicals in $[M^{II}(bpy)(L\cdot)](PF_6)$ complexes. *Angew. Chem. Int. Ed.* **42**, 563–567 (2003).
42. Ray, K. *et al*. The electronic structure of the isoelectronic, square-planar complexes $[Fe^{II}(L)_2]^{2-}$ and $[Co^{III}(L^{Bu})_2]^-$ (L^{2-} and $(L^{Bu})^{2-}$ = benzene-1,2-dithiolates): an experimental and density functional theoretical study. *J. Am. Chem. Soc.* **127**, 4403–4415 (2005).
43. Shupack, I., Billig, E., Clark, R. J. H., Williams, R. & Gray, H. B. The electronic structures of square-planar metal complexes. *vs.* spectral properties of the maleonitriledithiolate complexes of nickel, palladium, and platinum. *J. Am. Chem. Soc.* **86**, 4594–4602 (1964).
44. Sawyer, D. T., Srivatsa, G. S., Bodini, M. E., Schaefer, W. & Wing, R. M. Redox chemistry and spectroscopy of toluene-3,4-dithiol ($TDTH_2$) and of its $M(TDT)_2^{2-/-}$ complexes with zinc(II), copper(II), nickel(II), cobalt(II), iron(II), and manganese(II). Formation of a stable $d^n-(\cdot SR)$ bond upon oxidation by one electron. *J. Am. Chem. Soc.* **108**, 936–942 (1986).
45. Ray, K., Weyhermuller, T., Goossens, A., Craje, M. W. J. & Wieghardt, K. Do S,S'-coordinated o-dithiobenzosemiquinonate(1−) radicals exist in coordination compounds? The $[Au^{III}(1,2\text{-}C_6H_4S_2)_2]^{1-/0}$ couple. *Inorg. Chem.* **42**, 4082–4087 (2003).
46. Szilagyi, R. K. *et al*. Description of the ground state wave functions of ni dithiolenes using sulfur k-edge x-ray absorption spectroscopy. *J. Am. Chem. Soc.* **125**, 9158–9169 (2003).
47. Sarangi, R. *et al*. Sulfur k-edge x-ray absorption spectroscopy as a probe of ligand−metal bond covalency: metal vs ligand oxidation in copper and nickel dithiolene complexes. *J. Am. Chem. Soc.* **129**, 2316–2326 (2007).
48. Balch, A. L. Electron-transfer series involving sulfur-rich, polynuclear iron dithiolene complexes. *J. Am. Chem. Soc.* **91**, 6962–6967 (1969).
49. Lemmen, T. H. & Kocal, J. A. Yip-Kwai Lo, F., Chen, M. W. & Dahl, L. F. Structural characterization of the $[Fe_4(S_2C_2(CF_3)_2)_4(.mu.3\text{-}S)_4]^{2-}$ dianion. Stereochemical relationship between the cubane like Fe_4S_4 cores of this Balch dithiolene dianion and the $[Fe_4(.eta.5\text{-}C_5H_5)_4(.mu.3\text{-}S)_4]^{2+}$ dication and resulting electronic implications. *J. Am. Chem. Soc.* **103**, 1932–1941 (1981).
50. Herskovitz, T. *et al*. Structure and properties of a synthetic analogue of bacterial iron–sulfur proteins. *Proc. Natl. Acad. Sci. USA* **69**, 2437–2441 (1972).
51. Scott, T. A. & Zhou, H.-C. The First All-Cyanide Fe_4S_4 Cluster: $[Fe_4S_4(CN)_4]^{3-}$. *Angew. Chem. Int. Ed.* **43**, 5628–5631 (2004).
52. O'Sullivan, T. & Millar, M. M. Synthesis and study of an analog for the $[Fe_4S_4]^{3+}$ center of oxidized high potential iron-sulfur proteins. *J. Am. Chem. Soc.* **107**, 4096–4097 (1985).
53. Depamphilis, B. V. *et al*. Synthetic analogs of the active sites of iron-sulfur proteins. VI. Spectral and redox characteristics of the tetranuclear clusters $[Fe_4S_4(SR)_4]^{2-}$. *J. Am. Chem. Soc.* **96**, 4159–4167 (1974).
54. Kanatzidis, M. G., Coucouvanis, D., Simopoulus, A., Kostikas, A. & Papaefthymiou, V. Synthesis, structural characterization, and electronic properties of the tetraphenylphosphonium salts of the mixed terminal ligand cubanes $Fe_4S_4(Et_2Dtc)_n(X)_{4-n}^{2-}$ (X = Cl^-, PhS^-) (n = 1, 2). Two different modes of ligation on the $[Fe_4S_4]^{2+}$ core. *J. Am. Chem. Soc.* **107**, 4925–4935 (1985).
55. Kanatzidis, M. G. & Coucouvanis, D. Addition of activated acetylenes to coordinated polysulfide ligands. 2. Synthesis of the $Fe_2[S_2C_2(COOCH_3)_2]_4^{2-}$ dithiolene complex by the addition of $CH_3OOCC{\equiv}CCOOCH_3$ to the $(Fe_2S_{12})^{2-}$ anion. The crystal and molecular structure of $(Ph_4P)_2Fe_2[S_2C_2(COOCH_3)_2]_4$. *Inorg. Chem.* **23**, 403–409 (1984).
56. Holm, R. H. Electron transfer: Iron-sulfur clusters. *Comprehensive coordination chemistry II* Ed. McCleverty, J. A. & Meyer, T. J. 61–90 (2005).
57. Nam, W. Cytochrome p450. *Comprehensive coordination chemistry II* Ed. McCleverty, J. A. & Meyer, T. J. 281–307 (2005).
58. Segal, B. M., Hoveyda, H. R. & Holm, R. H. Terminal ligand assignments based on trends in metal−ligand bond lengths of cubane-type $[Fe_4S_4]^{2+,+}$ clusters. *Inorg. Chem.* **37**, 3440–3443 (1998).
59. Carney, M. J., Papaefthymiou, G. C., Spartalian, K., Frankel, R. B. & Holm, R. H. Ground spin state variability in $[Fe_4S_4(SR)_4]^{3-}$. Synthetic analogs of the reduced clusters in ferredoxins and other iron-sulfur proteins: cases of extreme sensitivity of electronic state and structure to extrinsic factors. *J. Am. Chem. Soc.* **110**, 6084–6095 (1988).
60. Kutal, C. Photochemical conversion and storage of solar energy. *J. Chem. Educ.* **60**, 882–887 (1983).
61. Sheldrick, G. A short history of SHELX. *Acta. Cryst. A* **64**, 112–122 (2008).

Acknowledgements

A. B. thanks Department of Science & Technology, Government of India, for the award of DST-EMR project (EMR/2014/000246). The authors thank DST-Sophisticated Analytical Instruments Facility (SAIF) at All India Institute of Medical Sciences (AIIMS), New Delhi for SEM and TEM analysis.

Author Contributions

A.Begum and S.Sarkar designed and carried out most of the experiments. A.H.Sheikh and G.Moula carried out some of the experiments.

Additional Information

Supplementary information accompanies this paper at https://doi.org/10.1038/s41598-017-17121-7.

Competing Interests: The authors have no competing interests as defined by Nature Publishing Group, or other interests that might be perceived to influence the results and/or discussion reported in this paper.

Publisher's note: Springer Nature remains neutral with regard to jurisdictional claims in published maps and institutional affiliations.